EIS and corrosion behaviour of plasma sprayed layers of Al and AlCr6Fe2 on AZ91

Elektrochemická impedanční spektroskopie a korozní chování plazmově stříkaných vrstev Al a AlCr6Fe2 na AZ91

Kubatík F. T.[1], Stoulil J.[2], Lukáč F.[1]. Stehlíková K.[2], Slepička P.[3]
[1] Department of Materials Engineering, Institute of Plasma Physics CAS
[2] Department of Metals and Corrosion Engineering, University of Chemistry and Technology
[3] Department of Solid State Engineering, University of Chemistry and Technology
E-mail: kubatik@ipp.cas.cz

This work presents the preparation of coatings of aluminium and $AlCr_6Fe_2$ alloy on magnesium alloy AZ91 with metallurgical bonding. Coatings were prepared by plasma spraying system WSP®-H 500. This metallurgical bond (sub-layer) is formed by an eutectic structure consisting of the intermetallic phase $Mg_{17}Al_{12}$ and the solid solution of magnesium and aluminium. In this work, the layers were studied using electrochemical impedance spectroscopy (EIS). It was shown that there is a several fold increase of the polarization resistance (R_{CT}) of plasma-sprayed coatings of aluminium and AlCr6Fe2 alloy, compared with uncoated AZ91 in borate buffer with pH 9.1.

Tato práce prezentuje přípravu plazmových nástřiků hliníku a slitiny AlCr6Fe2 na hořčíkové slitině AZ91 s metalurgickou vazbou. Plazmové nástřiky byly připraveny plazmovým hořákem WSP®-H 500. Tato metalurgická vazba (sub-vrstva) je tvořena eutektickem tvořeným intermetalickou fází $Mg_{17}Al_{12}$ a tuhým roztokem hořčíku a hliníku. V této práci byly plazmové nástřiky studovány pomocí elektrochemické impedanční spektroskopie (EIS). Ukázalo se, že plazmové nástřiky hliníku a slitiny AlCr6Fe2 mají několikanásobné zvýšení polarizačního odporu (RCT) ve srovnání s nepovlakovaným substrátem hořčíkovou slitinou AZ91 v boritanovém pufru s pH 9,1.

INTRODUCTION

Magnesium alloys are promising materials for light-weight structures in automotive and aerospace industries due to their high specific strength and stiffness [1, 2]. The very poor corrosion resistance of magnesium and magnesium alloys considerably limits their wide application. Magnesium alloys are prone to galvanic corrosion, which may result in serious pitting corrosion attack, mainly in humid and salt environment [3-5]. The $Mg_{17}Al_{12}$ intermetallic phase is mostly present in the alloys with a great content of aluminium (AZ 91) [4, 6]. This phase is nobler than the solid solution of magnesium and it becomes a micro-cathode in aqueous solutions and causes greater corrosion attack [4]. Many publications [7-11] deal with the research on the $Mg_{17}Al_{12}$ phase from many aspects. It is a fragile phase with a cubic body centred lattice [7]. This phase is also corrosion resistant in the NaCl solution. Presence of the $Mg_{17}Al_{12}$ phase with a fine microstructure in magnesium alloys improves their corrosion resistance [8].

Magnesium and its alloys can be protected by surface layers. The technology of plasma spraying makes it possible to prepare metal (including metals with high melting point), ceramic, metal-ceramic coatings and functionally graded coatings consisting with two or more components [12-14]. Author Parco and al. [15] studied the influence of the surface condition of the substrate of magnesium alloy AZ 91, especially preheating temperature and surface roughness, on bonding mechanisms of plasma coatings of Al, Al_2O_3, and $NiAl_5$. Qian et al. [16] studies the corrosion properties, especially potentiodynamic measurement of plasma-sprayed coatings with layer thicknesses exceeding 400 mm, of $AlSi_{12}$ alloy on the AZ91 magnesium alloy. The corrosion rate was decreased almost 4 times to (0.19 mg cm^{-2} day^{-1}) of the coated alloy as compared to AZ91 without any coating (0.71 mg cm^{-2} day^{-1}) [16]. It was published [16] that the Al–Si plasma coating with subsequent laser remelting improved the coating adhesion strength due to the development of the $Mg_{17}Al_{12}$ sub-layer at the coating-substrate interface [16]. This work focuses on the study of the corrosion resistance of plasma-sprayed coatings of aluminium and AlCr6Fe2 aluminium alloy and studies the corrosion behaviour of characteristic sub-layers formed by $Mg_{17}Al_{12}$ intermetallic phase and by a solid solution of magnesium with aluminium (hereinafter referred to as sub-layer)[10] on the AZ91. Coatings were prepared by the hybrid water-stabilised plasma torch WSP-H 500. AlCr6Fe2 aluminium alloy is thermally

stable up to 300 °C [17, 18]. This paper describes the sub-layer formation during the plasma spraying of aluminium and AlCr6Fe2 on AZ91 substrates. The present work deals with measuring the electrochemical impedance spectroscopy of thin plasma-sprayed coatings, and with the characterization of the equivalent electrical circuit. Corrosion measurement is complemented by long-term corrosion tests of plasma sprayed coatings in humid environments. In this work a significant influence of the sub-layer on the corrosion resistance of protective coatings on the magnesium alloy AZ91 is revealed.

EXPERIMENTAL PART

In this research, two powders were used, in particular commercially pure aluminium Al powder (GTV, Germany) with grain size from -90 to +45 mm and aluminium alloy AlCr6Fe2 powder (UCT-Prague, Czech Rep.) with grain size from -180 to +80 mm. Chemical composition of the powders is given in Table 1. Plasma coatings were prepared by means of a hybrid water-stabilised plasma torch WSP®-H 500 with power of up to 160 kW. The powder was injected into the plasma jet by a carrier gas Ar+H_2 7 vol. %. Spraying distance of 350 mm was experimentally determined to be a distance when the powder is melted through, but it is not overheated or oxidised. In the research, layers were prepared with one and two passes on the substrates preheated to 180 °C. One pass represents one pass during plasma spraying on the substrate by a robot moving with the velocity of 300 mm/s. All the technological parameters of plasma spraying are given in Table 2. Substrates with the dimensions of 70×20×5 mm^3 were made from the AZ91 magnesium alloy (as-cast state) the substrate surface was ground with an abrasive paper with P-700 grain and degreased with acetone. The prepared specimens with plasma coatings were cut, and then their cross-sections were prepared. The cross-sections were observed by means of a scanning electron microscope Carl Zeiss SMT, EVO MA 15.

Sample phase composition was measured by X-ray diffraction in the standard Bragg-Brentano geometry with a divergent beam and with a beam knife placed above the samples in order to minimize the effects of air scattering. Since our aim was to further measure the centres of the sintered samples, the irradiated volumes were in the middle of the samples' cross-sections. Therefore, a poly-capillary system and a collimator of 1 mm in diameter were inserted into the primary X-ray beam path changing the originally divergent character into a quasi-parallel one; diffraction Cu-K radiation was detected with a 1D Lynx-Eye detector. The used D8 Discover diffractometer was equipped with a laser system and a compact *x*, *y*, *z* stage facilitating precise positioning of the measured surface.

The electrochemical impedance spectroscopic measurement was performed in a standard connection with three electrodes using the Gamry FAS 2 potentiostat in connection with Gamry corrosion measurement software. Borate buffer with pH 9.1 (0.075 M $Na_2B_4O_7$ + 0.05 M boric acid) was used as a corrosion medium. The exposed area of the specimen was 0.8 cm^2. The measurement was performed directly on the original plasma sprayed surface at the laboratory temperature within the range of 10 kHz – 10 mHz frequencies, at Eoc (open circuit potential); amplitude 10 mV; 5 points per decade. Laser Confocal Microscopy (LCM) images were taken under ambient conditions on an Olympus LEXT OLS 3100 microscope with the magnification up to 14400×. Objective lenses 5 – 100× with total magnification 120 – 14400× were used for the analysis (results from 10× objective are introduced in the paper). Laser confocal microscope uses a laser beam of wavelength 408 nm, with optical elements adapted for this short wavelength so that structures with resolution up to 120 nm laterally and in Z-axis 40 nm can be displayed precisely. The basic

Tab. 2. Atmospheric plasma spraying parameters. / *Parametry atmosférického plazmového stříkání*

Spraying parameters	Al, AlCr6Fe2
Arc voltage (V)	300
Arc current (A)	500
Flow rate of primary gas-protects the W-cathode (Ar) (L/min)	13
Flow rate of carrier gas (Ar+H) (L/min)	15
Rate of powder feeding Al (g/min)	110
Rate of powder feeding AlCr6Fe2(g/min)	170
Movement of spraying gun (mm/s)	300
Spraying distance (mm)	350

Tab. 1. Chemical compositions (in wt. %) of the used powders and AZ91 substrate. / *Chemické složení (hm. %) použitých prášků a substrátu AZ91*

	Al	Mg	Si	Zn	Fe	Cr	Mn	Cu
AZ 91	8.5	Bal.	0.05	0.54	0.003	–	0.20	0.002
Al	Bal.	–	0.08	–	0.11	–	–	0.001
AlCr6Fe2	Bal.	–	–	–	2.34	6.34	–	–

principle of confocal microscope is that it forms images point by point, by line scanning. Due to this procedure are therefore acquired optical cuts in X-Y plane and by precisely defined lens shift in the Z axis, the individual optical sections. Confocal images are always in focus and represent the individual optical cut of the sample. Composition of three-dimensional images is based on the possibility of progressive scan of tens to hundreds of optical sections in Z-axis and their combination. Without the short wavelength laser the „optical cutting" with high resolution would not be possible. Long-term corrosion tests were conducted in the MLW-WS-31 (GDR) condensation chamber according to the modified standard EN ISO 9227. Magnet was stuck on the backside of the specimens with the dimensions of 70×20×5 mm^3. The surfaces without plasma coating were protected with two-component epoxy resin S 1300 and transparent silicone. The non-coated AZ91 alloy was covered (masked magnet) in the same way. The samples with stuck magnets were vertically positioned on a support made from magnetic corrosion-resistant steel, which was placed in the chamber. The experiments were conducted at the temperature of 35 ± 3 °C, the specimens were exposed to 100% humidity. The specimens were weighted once a week for the total period of 504 hours (3 weeks). The results are plotted in the graph as mass gains related to the area depending on the oxidation time.

RESULTS AND DISCUSSION

Microstructure

Figure 1 shows the microstructures of the used powders (feedstock) Al and AlCr6Fe2. It can be seen that the used Al powder is of irregular shape, most often of longitudinal straight or twisted particles. The powder also contains small particles. Due to the powder structure, the feeding tubes clogged and therefore a smaller quantity of powder to be fed in was selected. The AlCr6Fe2 powder comprises of regular spherical particles. The surface of plasma coatings of Al, see Figure 2 (Al) comprises of classic "splats" as well as of small spherical particles (visible in the layer cuts). Such a surface is not suitable as a diffusion corrosion barrier. In the case of the plasma spraying of AlCr6Fe2, see Figure 2 (AlCr6Fe2), with greater size, the coating surface comprises of splats and porous structure. The XRD pattern of the Al and AlCr6Fe2 surface is seen in Figure 2. X-ray analysis of the surface of plasma sprayed Al confirms up to 36 % of Al_2O_3 (metastable phases cubic g and tetragonal d-Al2O3, whose structural data were taken from ICSD with codes 95302 and 40200 respectively) and fcc Al (code 43423). Despite the higher content of Al_2O_3, the effect on corrosion resistance of Al and AlCr6Fe2 plasma sprayed coatings was not observed. No partial barrier effect of Al_2O_3 splats on the oxygen diffusion was observed. This work has focused primarily on the corrosion resistance of the sub-layer (bonding layer), which has a major influence as a corrosion barrier. The phase identification revealed (surface of plasma sprayed AlCr6Fe2), the expected fcc (Fm3m) aluminium solid solution, and monoclinic (C12/m1) $Al_{45}Cr_7$ aluminium chromium phase (ICSD code of 57652). As a minor phase was detected a quasicrystalline phase of aluminium and transition metals, $Al_{95}Fe_4Cr$, which was identified by Manaila et al. [19] and due to the unknown

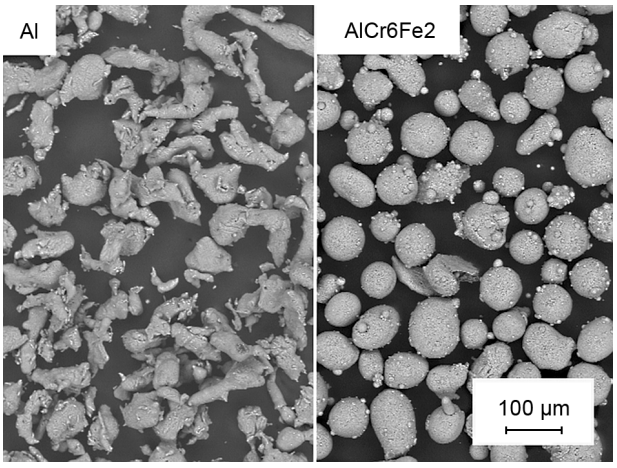

Fig. 1. Feedstock Al powder, fraction –90 +45 µm and AlCr6Fe2 powder, fraction –180 +80 µm (SEM-BSE)
Obr. 1. Podávané prášky Al prášek s frakcí -90 +45 µm a hliníková slitina AlCr6Fe2 s frakcí –180 +80 µm (SEM-BSE)

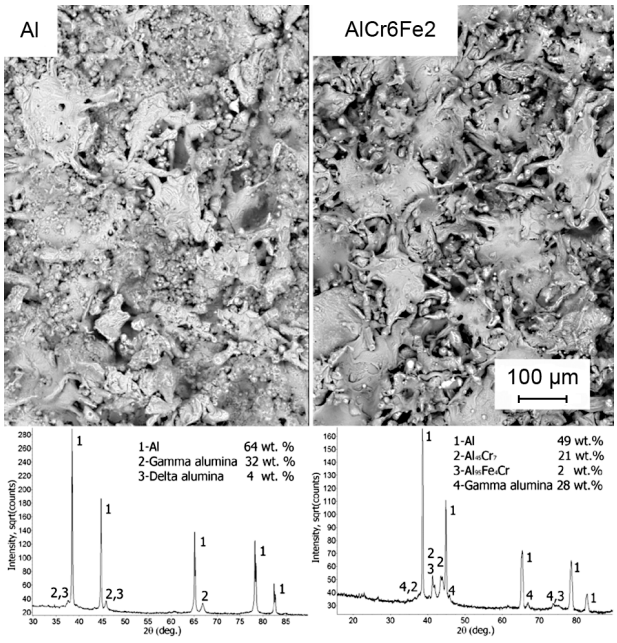

Fig. 2. Free-surface of plasma-sprayed Al and AlCr6Fe2 (SEM-BSE), with XRD-phase analysis
Obr. 2. Povrch plazmově stříkaného Al a AlCr6Fe2 (SEM--BSE), s RTG fázovou analýzou

atomic positions in this crystallographic structure was not involved in Rietveld quantitative analysis. In Figure 3, there are microstructures of the cuts of the specimens with the coatings with one and two passes for Al and AlCr6Fe2. When Al and AlCr6Fe2 powders are plasma sprayed, the surface of magnesium substrate becomes melted by the impact of melted particles. However, due to high thermal conductivity, the melted surface solidifies quickly while a sub-layer is created according to a binary Mg-Al diagram: $Mg_{17}Al_{12}$ intermetallic phase and a solid solution of magnesium with aluminium. Characteristic microstructure of this sub-layer is clearly visible in Figure 4. Sub-layers have a relatively large variation in thickness and in some places are discontinuous, this has significant influence on the local corrosion attack as subsequently shown in the corrosion tests. Coatings prepared by one pass create a discontinuous layer with different thickness and porosity. The layer prepared by plasma spraying of Al with one pass is formed predominantly by sub-layer containing $Mg_{17}Al_{12}$ phase and solid solution of magnesium and aluminium, see Figure 3a. In the case of plasma spraying with two passes, there is a continuous layer with a thickness of about 100 mm, however, the layer is also porous and does not create a compact diffusion protection barrier. Overview of thicknesses of the coating layers and the thickness of sub-layers are given in Table 3.

Tab. 3. Thickness of coatings of Al and AlCr6Fe2 plasma sprayed in one and two passes on the magnesium alloyAZ91 from Figure 3-6 / *Tloušťky vrstev plazmově stříkaného Al a AlCr6Fe2 s jedním a dvěma přejezdy na hořčíkové slitině AZ91 z obr. 3-6*

	Al 1-pass	**Al 2-passes**	**AlCr6Fe2 1-pass**	**AlCr6Fe2 2-passes**
Sub-Layer	128 µm ±24	64 µm ±19	61 µm ±19	61 µm ±12
Top-Layer	none	98 µm ±30	52 µm ±22	131 µm ±15

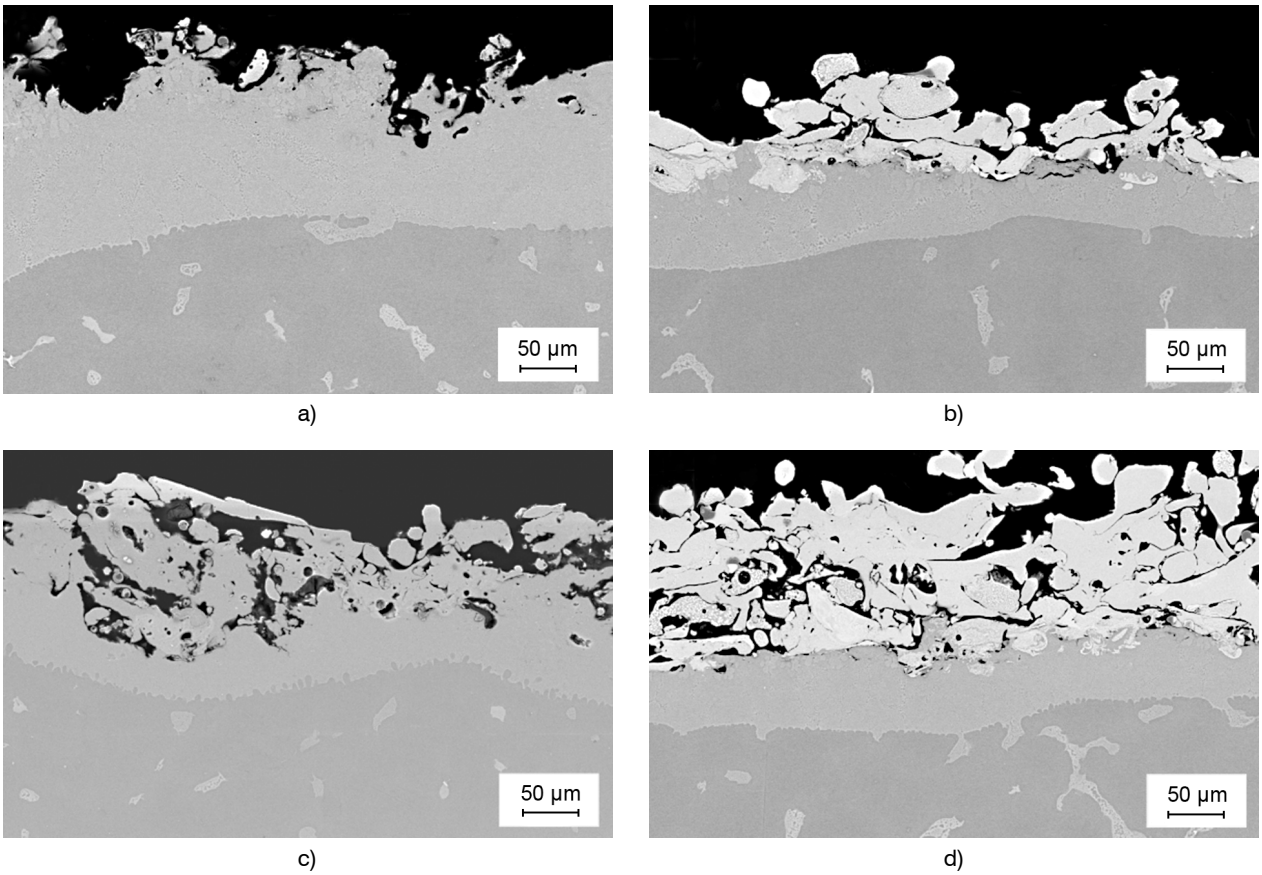

Fig. 3. Microstructure on the cross-section of Al coating prepared by 1 pass (a), AlCr6Fe2 coating 1 pass (b), Al coating 2 passes (c), AlCr6Fe2 coating 2 passes (d); on AZ91, (SEM-BSE)
Obr. 3. Mikrostruktury řezů Al vrstvy připravené jedním přejezdem (a), AlCr6Fe2 vrstvy jeden přejezd (b), Al vrstvy se dvěma přejezdy (c), AlCr6Fe2 vrstvy se dvěma přejezdy (d) na AZ91 (SEM-BSE)

The development of such sub-layers can be observed in the case of both Al and AlCr6Fe2 coatings [10]. The thickness of this sub-layer can be controlled: mainly with the substrate pre-heating temperature, in a smaller extent with the sprayed powder temperature as well as the quantity of the feed powder [10]. The $Mg_{17}Al_{12}$ phase is nobler [4] and the development of sub-layers and their structure affects the corrosion resistance.

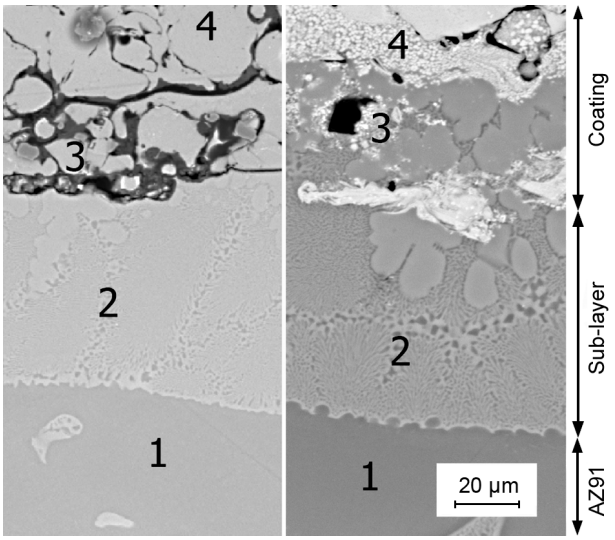

Fig. 4. Details (SEM-BSE) of bonding microstructure between Al (a) and AlCr6Fe2 (b) coatings and AZ91 substrate (results of the EDX analysis of the selected areas are in Tab. 4)

Obr. 4. Detail metalurgické vazby (SEM-BSE) mezi Al vrstvou (a) a AlCr6Fe2 vrstvou (b) a substrátem AZ91 (výsledky EDX analýzy označených oblastí jsou uvedeny v Tab. 4)

Tab. 4. Elemental analysis (at.%) in selected areas of Al coating 4A, AlCr6Fe2 coating 4b) on AZ91 / *Prvková analýza (at. %) označených obrastí z Obr. 4 a) Al vrstva a b) AlCr6Fe2 vrstva na substrátu AZ91*

Spot	Coating	Mg	Al	Cr	Fe	Zn	O
1	Al	86.8	9.2	–	–	0.8	3.3
2	Al	65.9	30.5	–	–	0.3	3.4
3	Al	49.9	42.9	–	–	–	7.2
4	Al	6.6	89.2	–	–	–	4.2
1	AlCr6Fe2	89.2	8.1	–	–	0.7	2.0
2	AlCr6Fe2	66.4	30.5	–	–	0.9	2.2
3	AlCr6Fe2	43.6	45.8	5.2	2.2	0.6	2.7
4	AlCr6Fe2	4.7	87.9	4.0	1.4	–	2.5

Details of bonding microstructure between Al and AlCr6Fe2 coatings and AZ91 substrate are visible in Figure 4. The figure also shows points of local EDX microanalysis. Results of the EDX microanalysis are presented in Table 4. EDX analysis for both sub-layers is very similar and shows ~66 at. % of Mg, and ~31 at.% of Al. According to the binary phase diagram, this corresponds to a mixture of the $Al_{12}Mg_{17}$ phase and solid solution of magnesium with aluminium. The point elemental analysis reveals a considerable diffusion of magnesium into the plasma coatings, see Figure 4. EDX microanalysis confirmed the presence of 4 at. % of Mg in the AlCr6Fe2 plasma coating ~10 mm away from the sub-layer. Al plasma coating also contains of up to 6 at.% of Mg at the distance of ~40 mm away from the sub-layer.

Electrochemical corrosion test

Electrochemical impedance spectroscopy (EIS) is an experimental method that can determine the electrochemical characteristics of the studied system. Plasma coatings have a high porosity, large contoured surface and they are not homogeneous. To obtain the best results from measurements of EIS, this work utilizes a modern technology represented by ultraviolet laser scanning system to determine the real surface of plasma coatings.

Electrochemical impedance spectroscopy

The measurement by electrochemical impedance spectroscopy was made directly on the surface of plasma coatings. For the most accurate measurement of the actual surface an ultraviolet laser scanning system was applied. The plasma-sprayed coating features a large surface; therefore, the ratio of the real area was measured by laser confocal microscope, the results of the measurement are given in Table 5. For the electrochemical measurement, a borate buffer, to reduce the corrosion of porous plasma coatings as far as possible and determine the equivalent circuit for EIS measurements. Bode's diagrams are in Figure 5. They are illustrate two characteristic measurements for Al with 1 pass and AlCr6Fe2 coatings with 2 passes. Al coating with 1 pass consists predominantly sub-layer with a few Al splats, which do not form a continuous layer is visible in Figure 3a. AlCr6Fe2 coating 2 passes has a thickness of about 130 mm, includes a porosity. Fitting parameters are summarized in Table 5 from the Bode's diagrams. Figure 6 shows a Nyquist diagram displaying the dependence of the imaginary component of impedance on the real component of the impedance for all measured frequencies. The impedance increases for two passes for both the Al and AlCr6Fe2 coatings. Experimental results of EIS measurements have physical basis (see from Fig. 6) using a model of the electrical equivalent circuit with two R-C members [20]. A similar equivalent

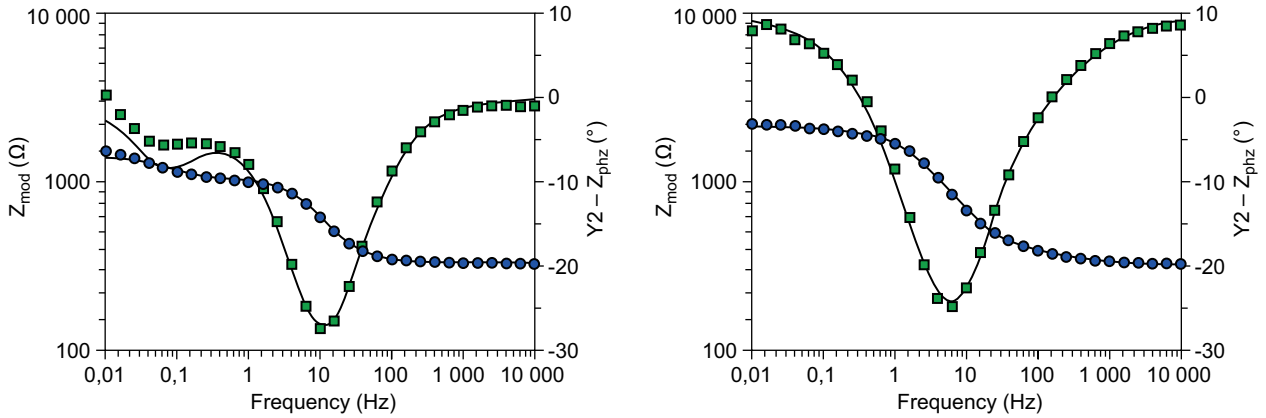

Fig. 5. Bode plots of Al (1 pass) and AlCr6Fe2 (2 passes) plasma coatings in a solution of borate buffer
Obr. 5. Bodeho diagramy plazmových nástřiků Al (1 přejezd) a AlCr6Fe2 (2 přejezdy) na hořčíkové slitině AZ91 v roztoku borátového pufru

Tab. 5. The parameters of impedance spectra fitting for coatings of Al and AlCr6Fe2 on magnesium alloy AZ91in borate buffer solution / . *Parametry fitování z impedančního měření vrstev Al a AlCr6Fe2 na hořčíkové slitině AZ91 v roztoku borátového pufru*

	Ratio of the laser measured surface versus geometric surface	**R_{SOL}**	**R_{CT}**	**R_{POR}**	**C_C**	**C_{DL}**
		(Ω)	(Ω)	(Ω)	($S.s^{\alpha}$)	($S.s^{\alpha}$)
AZ 91	1	316	275	836	4.96E-06	5.55E-05
Al 1 pass	9,2	331	22	4200	7.48E-05	1.002
Al 2 passes	10,2	335	135	2663	1.21E-04	4.73E-02
AlCr6Fe2 1 pass	18	227	68	4268	3.99E-04	4.26E-02
AlCr6Fe2 2 passes	15,7	329	89	6413	3.41E-04	1.97E-02

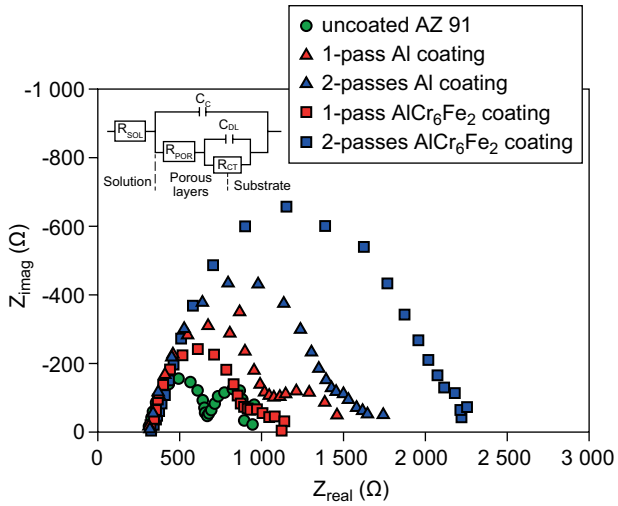

Fig. 6. Nyquist diagram of Al and AlCr6Fe2 plasma coatings and uncoated AZ91 in a solution of borate buffer, with equivalent circuit model used for the EIS data interpretation
Obr. 6. Nyquistův diagram pro Al a AlCr6Fe2 plazmové nástřiky a nepovlakovaný substrát AZ91 v roztoku borátového pufru, s ekvivalentním obvodem použitým pro EIS interpretaci dat

circuit was also proposed by Wen at al.in their work [21] that focuses on the EIS corrosion measurements of magnesium alloy AZ-X (where X: 31, 61, 91) with dispersed phase of $Mg_{17}Al_{12}$. In this work, it was reported that the nobler phase $Mg_{17}Al_{12}$ induces micro-galvanic coupling and accelerates the corrosion rate of the solid solution in magnesium alloys of type AZ-X [21]. The suggested model consisted of solution resistance (R_{SOL}), resistance of solution in the pores (R_{POR}), charge transfer resistance (R_{CT}), corrosion products capacitance (C_C) and electrical double layer capacitance (C_{DL}). In Table 5, the values of electrochemical impedance parameters are given. It should be taken into account, the real surface is not known. The surface ratio value is only area of open superficial pores. The values of double layer capacitance (C_{DL}) shows what is the area of conductive substrate, and that it is much lower for plasma coatings, compared to bare AZ91. C_C value may sign the conductivity of corrosion products, also much lower on AZ91. When multiplied by area ratio, R_{CT} values are higher for Al coating with 1 pass, AlCr6Fe2 coating with 1 pass and AlCr6Fe2

coating with 2 passes, thus they provide good barrier effect, approx. 5 times. R_{POR} shows interesting behaviour of Al coating with 2 passes. From the values of the (C_{DL}) can be seen, that a porosity of the Al coating with 1 pass is less than Al coating with 2 passes. This fact is also confirmed by the observation of the microstructures in cross-section, see Figure 3b. However, the Al coating with 1 pass has an increased dissolution than Al coating with 2 passes.

Microstructure after Electrochemical corrosion test

All the coatings after the measurement were observed in the tested region by means of a scanning electron microscope (SEM with EDX analysis). In the case of the uncoated AZ91 shown in Figure 7, large extent of spot corrosion attack can be seen (EDX analysis in Fig. 7), which is characteristic for AZ91 containing a nobler intermetallic phase $Mg_{17}Al_{12}$ and a micro-galvanic couple is developed here. In the case of plasma-sprayed coatings with one pass, several regions of spot corrosion attack were observed. Figure 8 shows the surface of the plasma-coating of AlCr6Fe2 with one pass where characteristic local corrosion attack was observed with corrosion products containing Mg, Al and Cr from coating (EDX analysis in Fig. 8). The spot corrosion attack (shown by the arrow a) of the plasma coatings with two passes was observed in several cases and the corrosion damage had a structure similar to the one in Figure 8. Cross-sectional metallographic samples were prepared from samples after the EIS measurements (Fig. 9). Figure 9a depicts the Al plasma coating prepared with 1 pass: the microstructure has longitudinal cracks but the coating does not peel off. The plasma-sprayed coating of AlCr6Fe2 easily crack and peel off but does not significantly damage the sub-layer-see Figure 9. The 2-pass Al coating in Figure 9c has small longitudinal cracks in comparison with the coating of AlCr6Fe2. Even in the case of plasma-sprayed AlCr6Fe2 coating with two passes, Figure 9d shows that there is a detachment of the coating and also is obvious that the sub-layer is discontinuous, but due to the short exposure time during EIS measurements the corrosion attack does not occur. From the cross-sectional microstructure of the coatings, a place was found where the sub-layer is discontinuous and exhibits localized corrosion attack as documented in Fig. 10. In this small section, it is observed that the layer is completely peeled off and the sub-layer is not continuous and the point where the latter is not present point corrosion attack has occurred. The dark areas are the corrosion product of Mg and Al oxides with Cl content up to 5 wt. %, EDX analysis in Fig. 10. It can be seen that the corrosion continue through a solid solution of magnesium and aluminum and lighter phase $Mg_{17}Al_{12}$ of sub-layers are not damaged, corrosion exactly circumventing around the phase $Mg_{17}Al_{12}$.

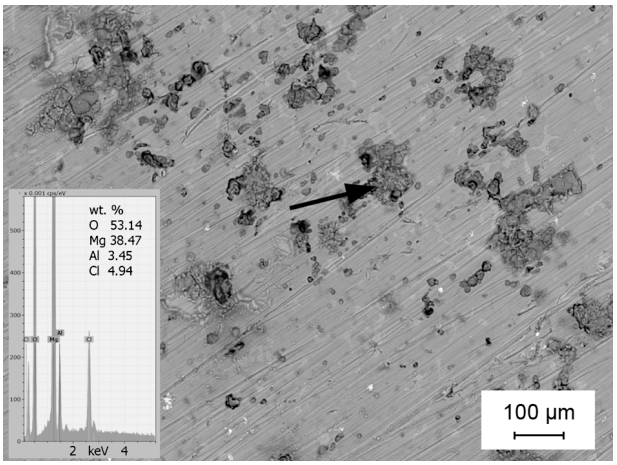

Fig. 7. Free-surface of AZ91after EIS measurements (SEM-BSE), with EDX analysis
Obr. 7. Povrch substrátu AZ91 po EIS měření (SEM-BSE), s EDX analýzou

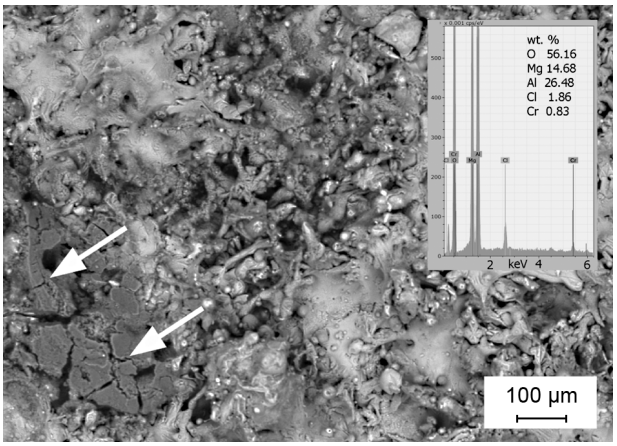

Fig. 8. Free-surface of AlCr6Fe2 coating (1 pass) on AZ91 after EIS measurements (SEM-BSE), with EDX analysis
Obr. 8. Povrch AlCr6Fe2 nástřiku (1 přejezd) na AZ91 po EIS měření (SEM-BSE), s EDX analýzou

Long-term corrosion tests

In most cases, the exposure time during the EIS measurement is too short for corrosion attack and indicated the positive influence of the sub-layers on corrosion resistance. Therefore, the EIS measurement was supplemented by the long-term corrosion experiments.

Environment of humid atmosphere

Figure 11 shows the plotted mass gain depending on exposure time in the humid atmosphere environment. It can be seen in the graph in Figure 11 that the uncoated AZ91 had the greatest mass gain – almost 2.5 g dm^{-2} after 504 hours. It is also evident in the graph that the coating of Al with one pass had the greatest mass gain of

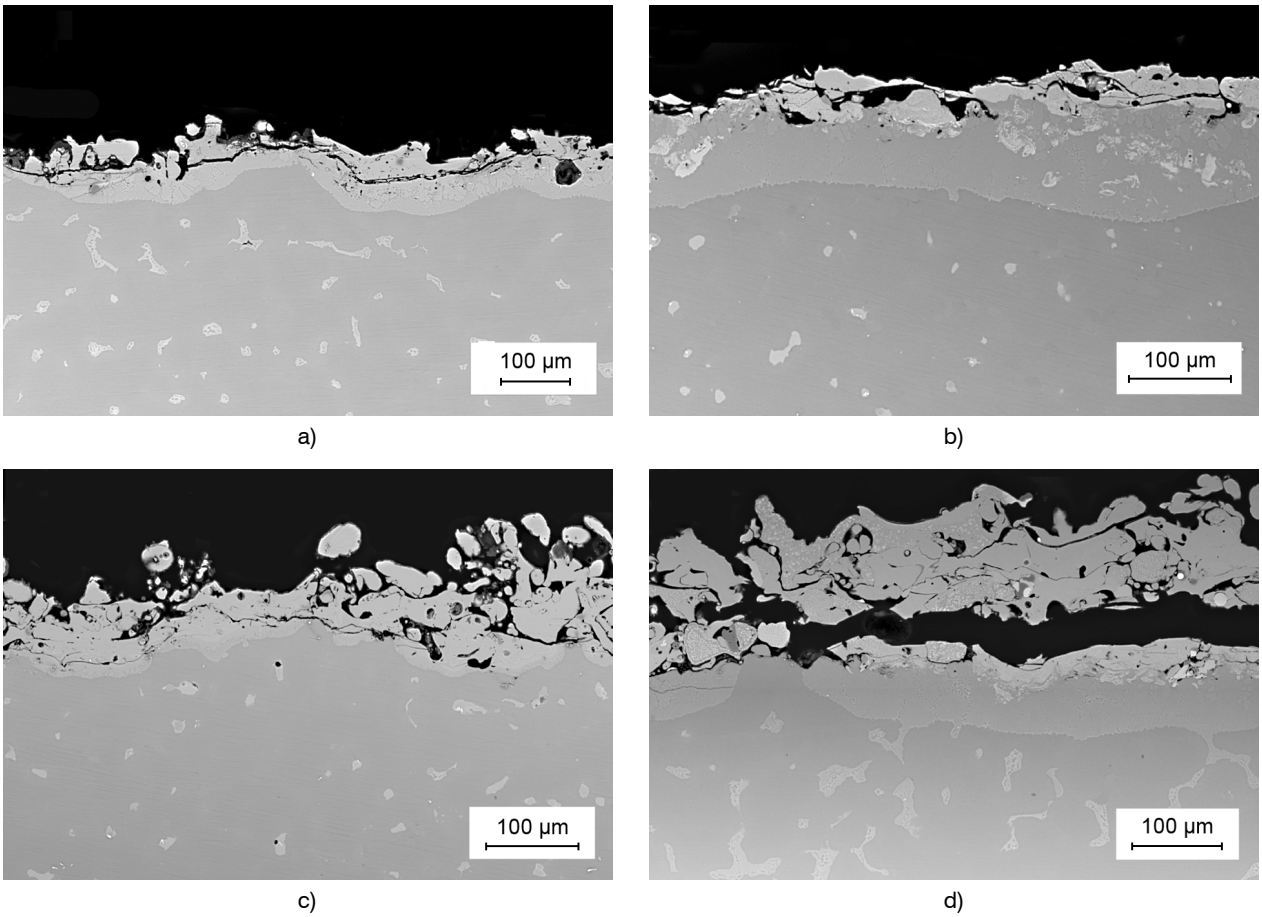

Fig. 9. Microstructure on the cross-section of Al coating prepared by 1 pass (a), AlCr6Fe2 coating, 1 pass (b), Al coating, 2 passes (c), AlCr6Fe2 coating, 2 passes (d) on AZ91 after EIS measurements (SEM-BSE).
Obr. 9. Mikrostruktury řezů vrstev Al nástřik (1 přejezd) (a), AlCr6Fe2 nástřik (1 přejezd) (b), Al nástřik (2 přejezdy) (c), AlCr6Fe2 nástřik (2 přejezdy) (d) na AZ91 po EIS měření (SEM-BSE)

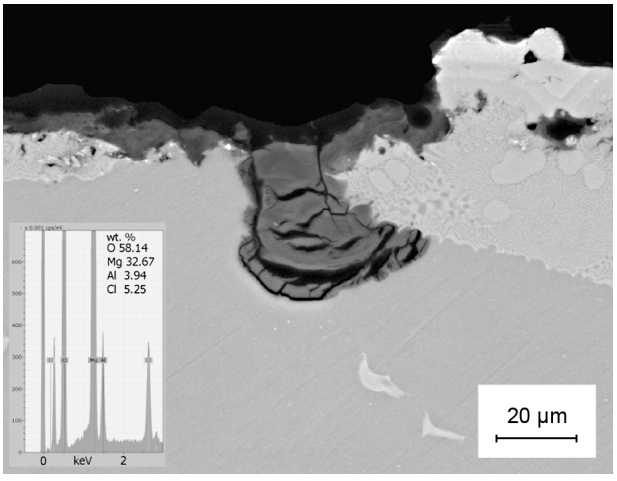

Fig. 10. Detail of corrosion attack, microstructure on the cross-section of AlCr6Fe2 coating, 1 pass on AZ91 after EIS measurements (SEM-BSE), with EDX analysis
Obr. 10. Detail korozního napadení, mikrostruktura řezu AlCr6Fe2 nástřiku, 1 přejezd na AZ91 po EIS měření (SEM--BSE), s EDX analýzou

all coated samples. The trend of slightly increasing mass gains can be observed in the case of other coatings. It can be seen from the graph that AlCr6Fe2 coatings have the lowest mass gains, the specimen with one pass has mass gain of 0.84 g dm^{-2} and the specimen with two passes has the mass gain of 0.63 g dm^{-2} after 504 hours. The coatings with two passes are thicker and have a better barrier effect observable already from the microstructures of coatings. This trend is also with compliance with the EIS measurement. Comparing R_{CT} decrease and mass gains of coated versus bare samples, we obtain similar four-fold increase in corrosion resistance of coated samples.

Microstructure after long-term corrosion tests

It is known from literature [6, 19] that AZ91 contains $Mg_{17}Al_{12}$ intermetallic phases, which are nobler and increase the corrosion rate of the solid solution of magnesium [19]: the oxidation rate around the nobler phase $Mg_{17}Al_{12}$ was increased due to galvanic corrosion, which resulted in a considerable point attack up to the depth of approx. 300 mm (Fig. 12 with EDX analysis).

The attention was focused on characteristic damages. Fig. 13 shows the free-surface of the plasma-sprayed coating with one pass of AlCr6Fe2 with characteristic spot attack formed by Mg and Al oxide (arrows b) (EDX analysis on Fig. 13). Such local corrosion attack is characteristic for both Al and AlCr6Fe2 coatings. In the centre of the spot, there is a large cluster of corrosion products of Mg and Al around it is the original splat structure of plasma coating. On the whole surface of the samples with plasma coatings of Al and AlCr6Fe2 prepared with one pass only one point appeared where there was a local corrosion attack and peel-off part of coating Fig. 14. With an increasing thickness of the corrosion products layer (arrow B) crevice corrosion expanded between the AlCr6Fe2 coating and the sub-layer, and its result was a peel-off of part of the coating (arrow C). The picture shows also the original plasma coating (arrow e with XRD-phase analysis shown in Fig. 16). Attention was focused on this corrosion damage, and their cross-sectional microstructure is shown in Figure 15. It is seen that if the sub-layer is continuous,

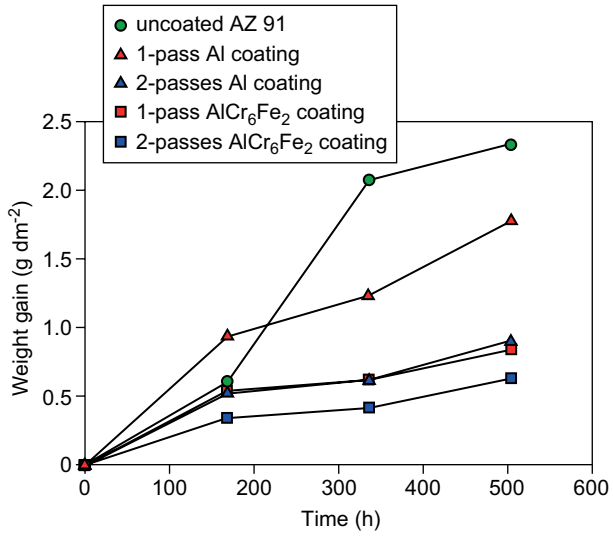

Fig. 11. The oxidation curves from long-term oxidation tests into condensation chamber at 35 °C, 100% humidity for hanged samples of plasma sprayed coatings of Al, AlCr6Fe2 and uncoated magnesium alloy AZ91

Obr. 11. Oxidační křivky z dlouhodobého oxidačního testu v kondenzační komoře při teplotě 35 °C, 100 % vlhkosti a vzorků zavěšených plazmově stříkaných Al a AlCr6Fe2 nástřiků a nepovlakované AZ91

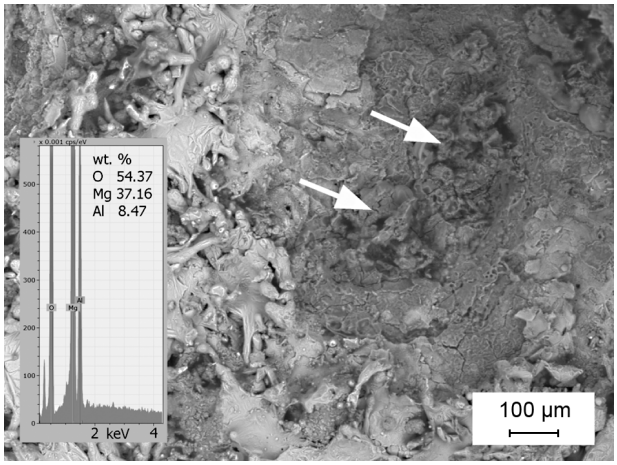

Fig. 13. Free-surface of AlCr6Fe2 coating (1 pass) on AZ91 after corrosion tests in environments of humid atmosphere at 35 °C, with characteristic local corrosion attack (SEM-BSE), with EDX analysis

Obr. 13. Povrch AlCr6Fe2 vrstvy (1 přejezd) na AZ91 po korozním testu v prostředí vlhké atmosféry při 35 °C, s charakteristickým lokálním korozním napadení (SEM-BSE), s EDX analýzou

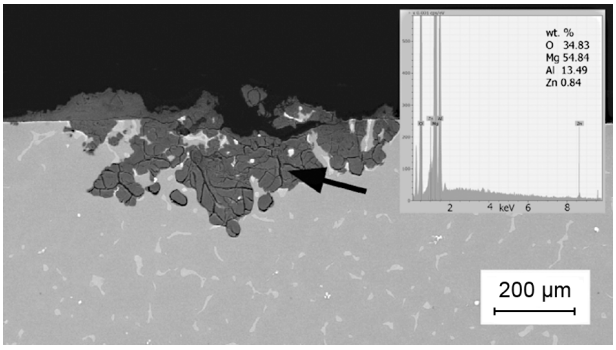

Fig. 12. Microstructure on the cross-section of uncoated magnesium alloy AZ91after corrosion tests in environment of humid atmosphere at 35 °C (SEM-BSE), with EDX analysis

Obr. 12. Mikrostruktura řezu nepovlakované hořčíkové slitiny AZ91 po korozním testu v prostředí vlhké atmosféry při 35 °C (SEM-BSE), s EDX analýzou

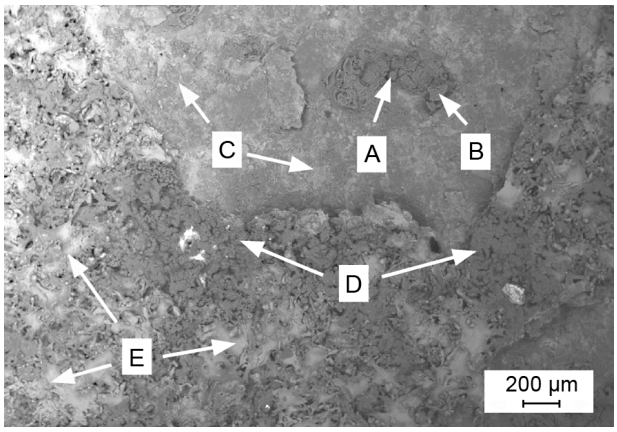

Fig. 14. Free-surface of AlCr6Fe2 coating (1 pass) on AZ91 after corrosion tests in environments of humid atmosphere at 35 °C, with damage of coating (SEM-BSE)

Obr. 14. Povrch AlCr6Fe2 vrstvy (1 přejezd) na AZ91 po korozním testu v prostředí vlhké atmosféry při 35 °C, s poškozením vrstvy (SEM-BSE)

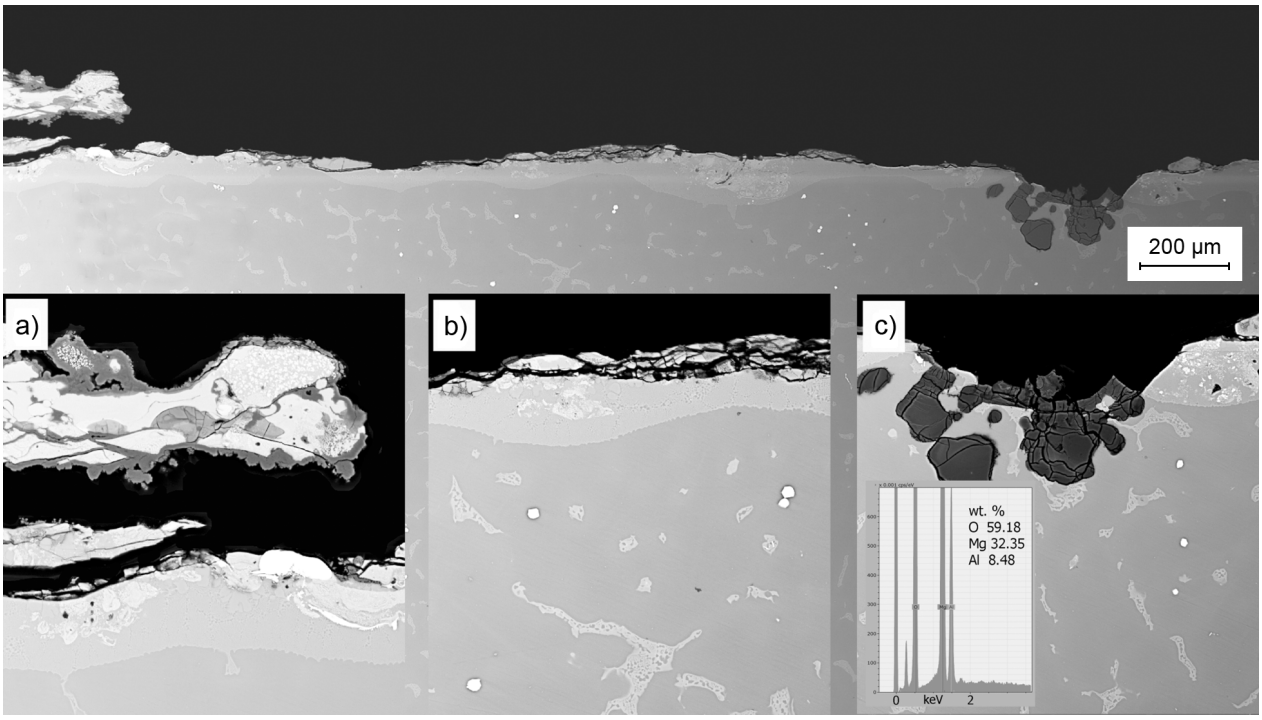

Fig. 15. Microstructure on the cross-section of AlCr6Fe2 coating on AZ91 after corrosion tests in environments of humid atmosphere at 35 °C (SEM-BSE), with EDX analysis
Obr. 15. Mikrostruktura řezu AlCr6Fe2 vrstvy na AZ91 po korozním testu v prostředí vlhké atmosféry při 35 °C, s poškozením vrstvy (SEM-BSE), s EDX analýzou

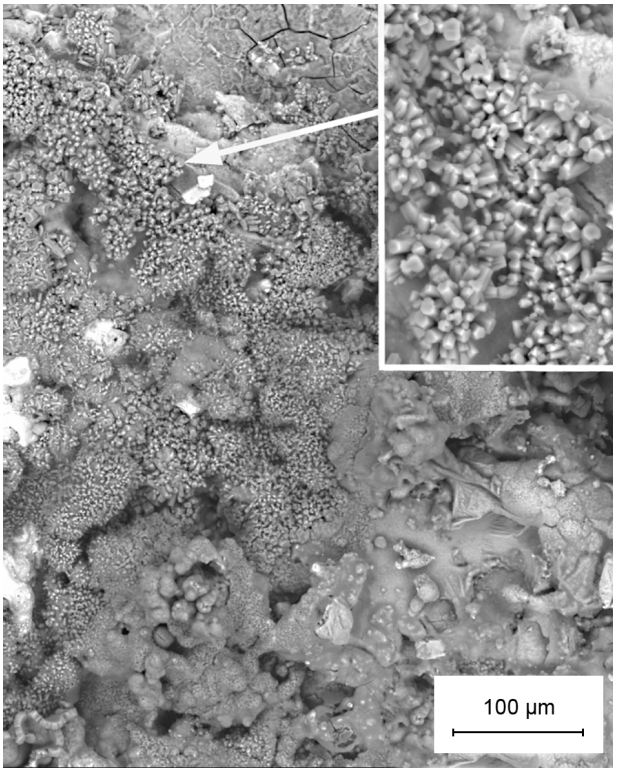

Fig. 16. Detail of free-surface of AlCr6Fe2 coating (1 pass) from Fig.14 (SEM-BSE)
Obr. 16. Detail povrchu AlCr6Fe2 vrstvy (1 přejezd) z Obr. 14 (SEM-BSE)

it serves as a good corrosion barrier. In the place where the sub-layer is broken or discontinuous, there is a local corrosion attack of the substrate AZ91, as shown in detail c), with EDS analysis in Fig. 15. In Figure 15a is a detail where it is seen that the original plasma coating peels off by the crevice corrosion and the peeled part of the layer is oxidized. By the observing the surface (arrow D) in Figure 14, it was found that the splats of aluminium alloy oxidize by galvanic corrosion i.e. the intermetallic phase $Al_{45}Cr_7$[17] in aluminium alloys are nobler and preferentially oxidized the solid solution of aluminium, and particles of intermetallic phases remain intact, as seen from the detail in Fig 16. In case that the sub-layer, it is intact and continuous, no local corrosion damage occurs by galvanic corrosion. In case of layer damage, corrosion of the solid solution of magnesium and aluminum occurs inside the cracks. Sealing of cracks is followed, by oxides of magnesium and aluminum, (Fig. 17, arrow A and B) and it is confirmed by EDX analysis. Fig. 17 shows a cross-section of the microstructure of the Al coating after 504 h of oxidation in a humid atmosphere. From the microstructure it can be seen that the plasma sprayed coating is cracked. Cracks across the sub-layer (indicated by arrow B) are sealed by corrosion products, but also an oval area of the original solid solution of magnesium and aluminium are corroded and filled with oxides of magnesium and aluminium as shown by the arrows A and EDX analysis in Figure 17.

Figure 18 shows a cross-sectional microstructure of the AlCr6Fe2 coating after 504 h oxidation in a humid atmosphere. The plasma-sprayed coating is cracked and, in some instances, cracks are sealed by oxides. Arrows indicate that individual splats of aluminium alloy are oxidized on the surface and form a barrier against further corrosion. EDX analysis in Figure 18 shows the chemical composition of the oxidized splats of coating formed by AlCr6Fe2.

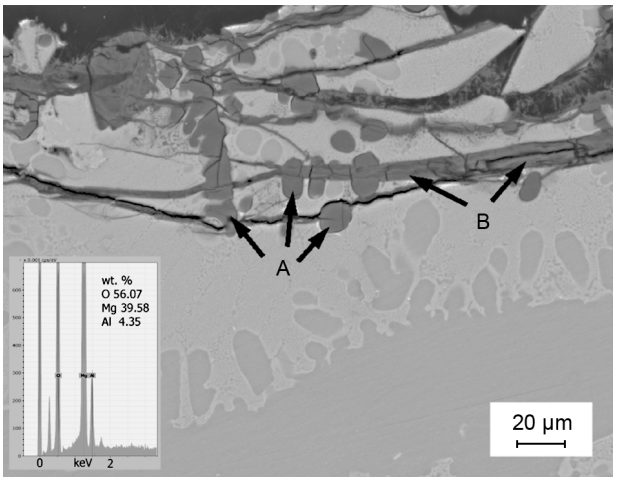

Fig. 17. Microstructure on the cross-section of Al coating (1 pass) on AZ91 after corrosion tests in environments of humid atmosphere at 35 °C (SEM-BSE), with EDX analysis
Obr. 17. Mikrostruktura řezu Al vrstvy (1 přejezd) na AZ91 po korozním testu v prostředí vlhké atmosféry při 35 °C (SEM-BSE), s EDX analýzou

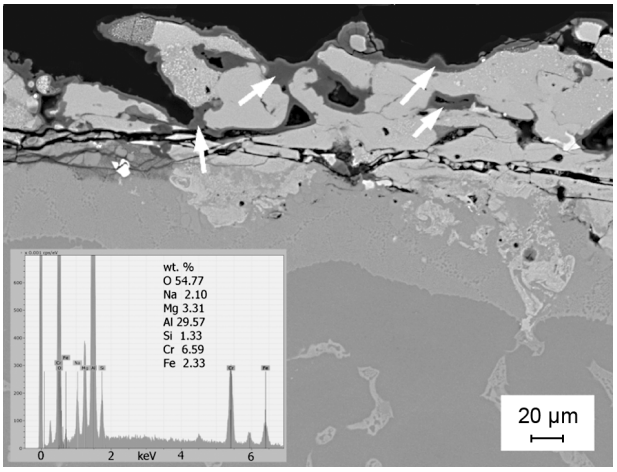

Fig. 18. Microstructure on the cross-section of AlCr6Fe2 coating (1 pass) on AZ91 after corrosion tests in environments of humid atmosphere at 35 °C (SEM-BSE), with EDX analysis
Obr. 18. Mikrostruktura řezu AlCr6Fe2 vrstvy (1 přejezd) na AZ91 po korozním testu v prostředí vlhké atmosféry při 35 °C (SEM-BSE), s EDX analýzou

CONCLUSION

In this research, plasma sprayed coatings of Al and AlCr6Fe2 were prepared with a plasma spraying system WSP®-H 500 on the substrate AZ91 magnesium alloy with pre-heating temperature of 180 °C. Along the substrate interface, the coatings form a metallurgic bond (sub-layer) with thicknesses from 61 to 128 mm, which is composed of $Mg_{17}Al_{12}$ phase and the solid solution of magnesium with aluminium. The Al coating prepared in one pass is not continuous and is formed previously by a sub-layer. The AlCr6Fe2 coating prepared in a one pass has a thickness of 52 mm. The coatings were prepared also with two passes with thicknesses of 98 mm for Al, and 131 mm for AlCr6Fe2. Both methods, EIS and long-term exposure test, showed good barrier properties of Al and AlCr6Fe2 coatings. The increase in corrosion resistance is approximately three-fold. It can be seen from the long-term corrosion tests in the humid atmosphere that the coatings prepared with two passes are without any visible changes even after 504 hours. The plasma-sprayed AlCr6Fe2 coating is prone to corrosion damage due to galvanic corrosion of solid solution of aluminium by nobler intermetallic phase $Al_{45}Cr_7$.

Acknowledgement

This work was supported by the Czech Science Foundation, project number 14-31538P "Evaluation of bonding interface during and after plasma spraying of metallic materials on magnesium and magnesium alloy."

REFERENCES

1. Mordike, B.; et al.: Magnesium. *Materials Scence and Engineering* **2001**, *302* (1), 37–45.
2. Eliezer, D.; et al.: Magnesium science technology and applications, *Advanced Performance Materials* **1998**, 3, 201–212.
3. Mathieu, S.; et al.: A corrosion study of the main constituent phases of AZ 91magnesium alloys. *Corrosion Science* **2003**, 45, 2741-2755.
4. Liu, Ch.; et al.: Study on biodegradation of the second phase $Mg_{17}Al_{12}$ in Mg–Al–Zn Alloys: In vitro experiment and thermodynamic calculation. *Materials Science and Engineering* **2013**, C 35, 1-7.
5. Dai, J.; et al.: Influences of alloying elements and oxygen on the stability and elastic properties of $Mg_{17}Al_{12}$. *Journal of Alloy and Compound* **2014**, 595, 142-147.
6. Bu, H.; et al.: Cold spray blended Al + $Mg_{17}Al_{12}$ coating for corrosion protection of AZ91D magnesium alloy. *Surface and Coating Technology* **2012**, 207, 155-162.
7. Ragani, J.; et al.: High-temperature deformation of the γ-$Mg_{17}Al_{12}$ complex metallic alloy, *Scripta Materialia* **2011**, 65, 253-256.

8. Kim, H.S.; et al.: Enhanced corrosion resistance of ultrafine-grained AZ61 alloy containing very fine particles of $Mg_{17}Al_{12}$ phase. *Corrosion Science* **2013**, 75, 228-238.
9. Lalpoor, M.; et al.: Nucleation mechanism of $Mg_{17}Al_{12}$-precipitates in binary Mg–7 wt. % Al alloy. *Journal of Alloy and Compounds* **2013**, 557, 73-76.
10. Kubatík, T.; F.; et al. Metallurgical bond between magnesium AZ91 alloy and aluminium plasma sprayed coatings. *Surface and. Coating Technology* **2015,** 282, 163-170.
11. Kannan, M.; B.; et al.: Biodegradability of β-$Mg_{17}Al_{12}$ phase in simulated body fluid. *Materials Letters* **2012**, 82, 54-56.
12. Hsiao, W.; T.; et al.: Wear resistance and microstructural properties of Ni–Al/h-BN/WC–Co coatings deposited using plasma spraying. *Materials Characterization* **2013**, 79, 84-92.
13. Wei, Q.; et al.: Oxidation control in plasma spraying NiCrCoAlY coating, *Applied Surface and Science* **2012**, 12, 5094-5099.
14. Parco, M.; et al.: Investigation of HVOF spraying on magnesium alloys. Surface and Coatings Technology **2006**, 201, 3269-3274.
15. Parco, M.; et al.: Investigation of particle flattening behaviour and bonding mechanisms of APS sprayed coatings on magnesium alloys. *Surface and Coatings Technology* **2007**, 201, 6290-6296.
16. Qian, M.; et al.: Corrosion performance of laser-remelted Al–Si coating on magnesium alloy AZ91D. *Corrosion Science* **2010**, 52, 3554-3560.
17. Kubatík, T.; F.; et al.: Compacting the powder of Al–Cr–Mn Alloy with SPS. *Materials and Technology* **2015**, 49, 129-132.
18. Bártová, B.; et al.: Structure and properties of rapidly solidified Al–Cr–Fe–Ti–Si powder alloys. *Journal of Alloy and Compounds* **2005**, 387, 193-200.
19. Manaila, R.; et al.: Icosahedral phases in the Al-Fe-Cr alloy system. *Physica Status Solidi A* **1988**, 109, 61-66.
20. Stoulil, J.; et al.: Thierry, Electrochemical properties of corrosion products formed on Zn–Mg, Zn–Al and Zn–Al–Mg coatings in model atmospheric conditions, *Materials Corrosion* **2015**, 66, 777-782.
21. Wen, Z.; et al.: Corrosion behaviours of Mg and its alloys with different Al contents in a modified simulated body fluid. *Journal of Alloy and Compounds* **2009**, 1, 392-399.